ADVANCED FUNCTIONAL MATERIALS
www.afm-journal.d

In Situ Photosynthesis of an $MAPbI_3$/CoP Hybrid Heterojunction for Efficient Photocatalytic Hydrogen Evolution

Cheng Cai, Yuan Teng, Jian-Hao Wu, Jun-Yan Li, Hong-Yan Chen,* Jing-Hua Chen, and Dai-Bin Kuang**

Halide perovskite like methylammonium lead iodide perovskite ($MAPbI_3$) with its prominent optoelectronic properties has triggered substantial concerns in photocatalytic H_2 evolution. In this work, to attain preferable photocatalytic performance, a $MAPbI_3$/cobalt phosphide (CoP) hybrid heterojunction is constructed by a facile in situ photosynthesis approach. Systematic investigations reveal that the CoP nanoparticle can work as co-catalyst to not only extract photogenerated electrons effectively from $MAPbI_3$ to improve the photoinduced charge separation, but also facilitate the interfacial catalytic reaction. As a result, the as-achieved $MAPbI_3$/CoP hybrid displays a superior H_2 evolution rate of 785.9 µmol h^{-1} g^{-1} in hydroiodic acid solution within 3 h, which is ≈8.0 times higher than that of pristine $MAPbI_3$. Furthermore, the H_2 evolution rate of $MAPbI_3$/CoP hybrid can reach 2087.5 µmol h^{-1} g^{-1} when the photocatalytic reaction time reaches 27 h. This study employs a facile in situ photosynthesis strategy to deposit the metal phosphide co-catalyst on halide perovskite nanocrystals to conduct photocatalytic H_2 evolution reaction, which may stimulate the intensive investigation of perovskite/co-catalyst hybrid systems for future photocatalytic applications.

1. Introduction

Hydrogen energy is an important clean source for replacing fossil fuels. Photocatalytic H_2 evolution from renewable solar energy is denoted as an effective approach to solve the global environmental and energy issues owing to the merits of utilizing the solar energy directly and the low energy consumption. Designing highly efficient and stable photocatalysts is currently vital for effective H_2 generation. On account of this, metal oxides,[1,2] sulfides,[3–5] C_3N_4,[6,7] halide perovskites,[8,9] etc. have been put to work as photocatalysts. In particular, lead-based halide perovskite (LHP) materials have obtained great interest in photovoltaics and optoelectronic applications due to their unique optical and electrical properties.[10–18] LHPs with appropriate band structures have also been developed as the photocatalytic materials for CO_2 reduction,[9,19] the oxidation of alcohols,[20] and particularly hydroiodic acid (HI) splitting.[8,21] As a promising example, methylammonium lead iodide perovskite ($MAPbI_3$) with wide light absorption range and excellent photoelectronic properties has been proved to be a good photocatalyst for hydrogen evolution reaction (HER). In 2016, Park et al. first reported the $MAPbI_3$ as a photocatalyst for the solar-driven splitting of HI solution,[8] which stimulates the photocatalytic application of halide perovskite-based materials.[21–34] For instance, Wu et al. constructed a $MAPbI_3$/rGO composite using facile photoreduction method, and achieved a much higher photocatalytic HI splitting efficiency than the pristine $MAPbI_3$ due to the efficient extraction of photogenerated electrons by rGO.[21] Wang et al. reported a Pt/TiO_2-$MAPbI_3$ composite by hybriding $MAPbI_3$ with Pt/TiO_2 which can greatly enhance the charge separation of $MAPbI_3$.[22] Most recently, Ni_3C-decorated $MAPbI_3$ composite and black phosphorus-anchored $MAPbI_3$ (BP/$MAPbI_3$) heterostructure have been constructed as well, and both of them exhibited remarkable photocatalytic H_2 activity.[24,25]

However, most of the reported works were mainly focused on large size (about tens of microns) LHP microcrystal materials, which possess limited active sites, and the photogenerated charge carriers must transport long distance to perform the photocatalytic reaction. In comparison, halide perovskite nanocrystals have large specific surface area and short carrier diffusion length, which may exhibit large potential in the field of photocatalysis application.[9,35–48] Encouragingly, in 2017, we for the first time reported a photocatalytic CO_2 reduction reaction by $CsPbBr_3$ QDs/graphene oxide composite in the non-aqueous ethyl acetate reaction media.[9] Subsequently, various lead-free perovskite nanocrystals including $Cs_2AgBiBr_6$,[19] Cs_2PdBr_6,[39] and $Cs_4CuSb_2Cl_{12}$[40] with tunable band gap were

---

C. Cai, Dr. Y. Teng, J.-H. Wu, J.-Y. Li, Dr. H.-Y. Chen, J.-H. Chen,
Prof. D.-B. Kuang
MOE Key Laboratory of Bioinorganic and Synthetic Chemistry
Lehn Institute of Functional Materials
School of Chemistry
Sun Yat-sen University
Guangzhou 510275, P. R. China
E-mail: tengy6@mail.sysu.edu.cn; chenhy33@mail.sysu.edu.cn;
kuangdb@mail.sysu.edu.cn

The ORCID identification number(s) for the author(s) of this article can be found under https://doi.org/10.1002/adfm.202001478.

DOI: 10.1002/adfm.202001478

synthesized to perform photocatalytic CO_2 reduction/photoelectrochemical cell application. Furthermore, various perovskite nanocrystal-based composite materials such as $CsPbBr_3$@metal oxides,[41] $CsPbBr_3$/Pd,[42] $CsPbBr_3$@metal-organic frameworks,[43,44] Cs_2SnI_6/SnS_2[45] as well as Fe_2O_3/RGO/$CsPbBr_3$ Z-scheme heterojunction[46] have been designed for improving photogenerated charge carrier separation and hence enhancing the photocatalytic performance.

In addition to regulating the size or the composition of catalysts, the introduction of co-catalysts is an another effective strategy to improve the photocatalytic performance, which can work as electron sinks and provides effective proton-reduction reaction sites.[42,47–53] As a typical example, cobalt phosphide (CoP) is an ideal candidate for constructing advanced hybrid catalysts due to its outstanding intrinsic activity and superior conductivity; and exciting progress has been obtained in the field of electrocatalytic H_2 evolution.[54–61] Although the pristine CoP exhibits negligible photocatalytic activity for H_2 evolution,[62] the integration of CoP as co-catalyst can help accelerate the photoelectron transfer and separation, and also reduce the reaction energy barrier effectively.[63–65] Hence, combining halide perovskite nanocrystals with CoP co-catalyst could significantly enhance the photocatalytic H_2 generation activity. However, it remains a big challenge to anchor metal phosphide co-catalyst on the surface of halide perovskite nanocrystal because of the compatibility and differences in preparation conditions of the two kinds of materials.

Herein, we devised the synthesis of a $MAPbI_3$/CoP hybrid heterostructure by a facile in situ photosynthesis strategy. The CoP co-catalyst was found to effectively extract the photoinduced electrons from $MAPbI_3$ nanocrystals to participate in the photocatalytic reaction, which contributed to a boosted photocatalytic H_2 evolution performance. As a consequence, the as-prepared $MAPbI_3$/CoP hybrid exhibited a better photocatalytic H_2 evolution performance compared with the $MAPbI_3$. The H_2 evolution rate of the $MAPbI_3$/CoP hybrid in 3 h of reaction was 785.9 μmol h^{-1} g^{-1}, which is 8.0 times higher than that of $MAPbI_3$ alone. Photoluminescence (PL), time-resolved photoluminescence (TRPL), electrochemical impedance spectroscopy (EIS), and Kelvin probe force microscopy (KPFM) were performed to characterize the photogenerated charge carriers separation and transportation. The results strongly indicate that the current $MAPbI_3$/CoP hybrid heterojunction is a promising catalyst for effective photocatalytic H_2 evolution.

2. Results and Discussion

The fabrication process of the $MAPbI_3$/CoP hybrid heterojunction is displayed in **Scheme 1**. Concretely, the $MAPbI_3$ nanocrystal (denoted as pristine $MAPbI_3$) was first prepared by the microcrystalline-assisted antisolvent method. And then, the $MAPbI_3$/CoP hybrid was synthesized by the in situ photodeposition process in which $CoCl_2$ and $NaHPO_2$ were dissolved in $MAPbI_3$-saturated HI solution to work as the precursor solution (see Experimental Section for details). Scanning electron microscopy (SEM) measurement was applied to determine the micro/nano-morphology of pristine $MAPbI_3$ and $MAPbI_3$/CoP samples, as displayed in Figure S1, Supporting Information. It can be clearly seen that both pristine $MAPbI_3$ and $MAPbI_3$/CoP hybrid exhibit a cube-like morphology, but the hybrid possesses a larger average size of ≈180 nm compared with pristine sample (≈90 nm), which could be ascribed to the ripening growth of $MAPbI_3$ nanocrystals during the photodeposit process of CoP. The powder X-ray diffraction (XRD) patterns of samples (**Figure 1**a) show that the bare $MAPbI_3$ exhibits a

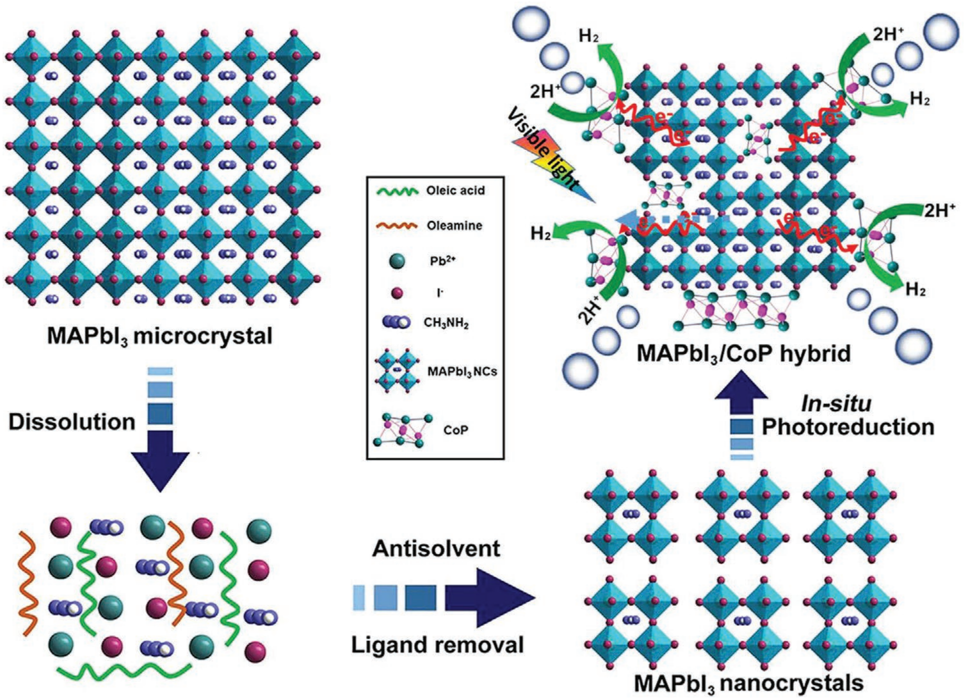

Scheme 1. Schematic diagram of the fabrication and photocatalytic H_2 evolution process of the $MAPbI_3$/CoP hybrid heterojunction.

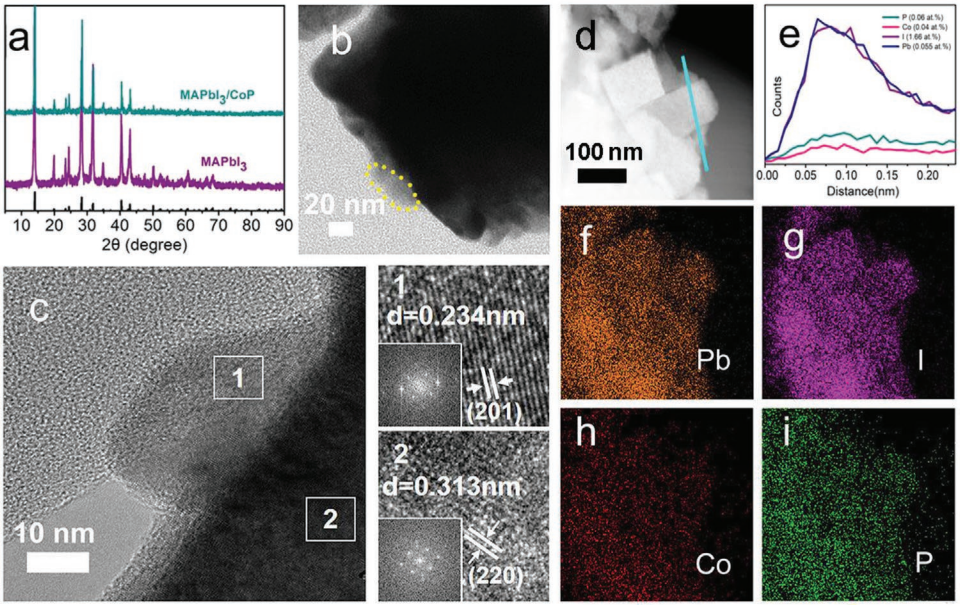

Figure 1. a) XRD patterns of pristine $MAPbI_3$ and $MAPbI_3$/CoP hybrid. b,c) The TEM and HRTEM images of $MAPbI_3$/CoP. d,e) HAADF-STEM image, line scan spectrum of $MAPbI_3$/CoP and the corresponding elemental mappings of f) Pb, g) I,h) Co, and (h) P.

tetragonal crystal structure with a space group of I4/mcm (ICSD card No. 250739), which matches well with the previous reports.[20,23,66,67] No peaks of CoP are observed in the XRD pattern of the $MAPbI_3$/CoP hybrid, which could be attributed to its relatively low content. Further transmission electron microscopy (TEM) image also confirms the cube-like morphology of $MAPbI_3$ (Figure S2a, Supporting Information). High-resolution TEM (HRTEM) image (Figure S2b, Supporting Information) clearly reveals the lattice fringe spacing of 0.312 nm, corresponding to the (220) plane of $MAPbI_3$. After the photodeposition of CoP, the morphology of the $MAPbI_3$/CoP sample is similar to that of pristine $MAPbI_3$ except for some fine particles that can be observed on the surface of $MAPbI_3$ (Figure 1b). HRTEM image (Figure 1c) exhibits two kinds of lattice fringe with interplanar spacings of 0.313 and 0.234 nm, corresponding to the (220) plane of $MAPbI_3$ and the (201) plane of CoP,

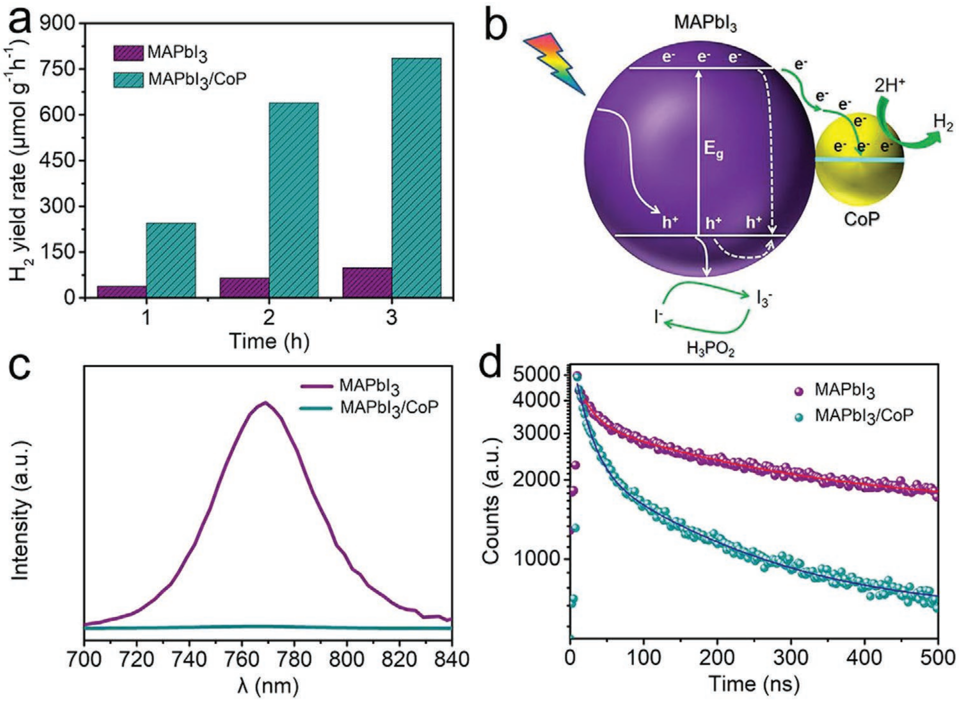

Figure 2. a) Photocatalytic HER performance under visible-light illumination ($\lambda \geq 420$ nm) of pristine $MAPbI_3$ and $MAPbI_3$/CoP hybrid. b) Schematic illustration of the photocatalytic HER process over the $MAPbI_3$/CoP hybrid. c) The corresponding PL and d) PL decay spectra.

respectively. These results indicate that the $MAPbI_3$/CoP hybrid heterojunction has been constructed successfully. High-angle annular dark-field scanning TEM (HAADF-STEM) image, element mapping, and line scan element analysis of the hybrid were also measured. As displayed in Figure 1d–i, the Pb, I, Co, and P elements are homogeneously distributed on the hybrid. However, the Co and P elements exhibit a sparse point-like distribution, which also implies the low content. Further proof comes from the energy-dispersive X-ray spectroscopy (EDX) result which also shows that the atomic percent of Co and P is quite low (Figure S3, Supporting Information). Furthermore, the optical properties of as-prepared samples were studied by the ultraviolet–visible (UV–vis) diffuse reflectance spectra. As shown in Figure S4, Supporting Information, the visible-light absorption spectrum of the $MAPbI_3$/CoP hybrid is slightly broadened than that of pristine $MAPbI_3$. This could be attributed to the increased particle size during the photosynthesis deposition process of CoP, which is in good agreement with the SEM results.

The photocatalytic HER activity of the as-prepared $MAPbI_3$/CoP hybrid was investigated in saturated aqueous HI solution under visible-light illumination. **Figure 2**a shows the photocatalytic HER activities of the $MAPbI_3$ and $MAPbI_3$/CoP samples. It can be seen that pristine $MAPbI_3$ possesses a photocatalytic HER rate of 97.8 μmol g^{-1} h^{-1} in 3 h of photocatalytic reaction. After photodeposition of CoP, the photocatalytic HER rate (785.9 μmol g^{-1} h^{-1}) is ≈8.0 times higher than that of pristine $MAPbI_3$, which is profited from the formation of the $MAPbI_3$/CoP heterojunction. Figure 2b illustrates the relative energy band position of $MAPbI_3$ and CoP, which forms a stepped path for electron transfer. When irradiated by visible light, the photogenerated electrons in the conduction band (CB) of $MAPbI_3$ could be extracted rapidly by the CoP nanoparticles, which can effectively facilitate the charge separation and inhibit the radiation recombination. Furthermore, the semi-metallic CoP nanoparticles, as a good electrocatalyst for HER, can also provide more reaction active sites (Figure S5, Supporting Information) and help to accelerate the HER. As a result, the photocatalytic performance of $MAPbI_3$/CoP can be largely enhanced. It should be noted that a proper loading amount of CoP is significant to achieve improved photocatalytic performance. As displayed in Figure S6, Supporting Information, the photocatalytic H_2 evolution performances of the $MAPbI_3$/CoP hybrids increase at first and then decrease when continuously increasing the loading amount of CoP, and the $MAPbI_3$/CoP sample prepared at theoretical feeding mass ratio of 1:0.25 exhibits the best performance. This is because proper amount of CoP nanoparticles can facilitate the transfer and separation of photoinduced charge carriers, but the excess loading amount of CoP would also act as the charge recombination centers, which would lead to a decreased catalytic performance.[68]

To further understand the positive effects of CoP on the catalytic performances of hybrid catalyst, the corresponding charge transfer and separation behaviors in $MAPbI_3$/CoP hybrid were investigated in detail. First, the steady-state PL spectrum was conducted to monitor the radiative recombination process of photoexcited charge carriers. Generally, a dramatically quenched PL signal is regarded as an indicator of effective charge transfer in the composite catalysts. As displayed in Figure 2c, the pristine $MAPbI_3$ shows a strong emission peak due to its high electron–hole recombination efficiency. After decorating with CoP, the emission peak almost disappears. Apparently, the introduction of CoP provides fast transfer paths for excited-state electrons of $MAPbI_3$, which can facilitate the charge separation and inhibit the radiative recombination. To obtain more details about the decay behavior of photogenerated carriers of as-prepared catalysts, TRPL spectra was also measured and fitted with a biexponential function,[21,25] as shown in Figure 2d and Table S1, Supporting Information. Obviously, the PL signal of $MAPbI_3$/CoP hybrid shows a faster decay rate than that of pristine $MAPbI_3$. According to the fitting results, the average PL lifetime (τ_{avg}) of $MAPbI_3$/CoP (148.1 ns) is much shorter than that of pristine $MAPbI_3$ (232.6 ns). Specifically, the contribution of τ_1 (fast decay component, related to electron transfer) increases largely from 5.77% for $MAPbI_3$ to 14.44% for $MAPbI_3$/CoP. This result further confirms the conclusion that the introduction of CoP can accelerate the photogenerated electron transfer from $MAPbI_3$ to CoP which inhibits the radiative recombination largely.

To further clarify the origin of high HER activity of the $MAPbI_3$/CoP hybrid, optoelectrochemical performance of photocatalysts associated with photogenerated charge transfer and separation were characterized and analyzed by transient photocurrent responses and EIS measurement. **Figure 3**a

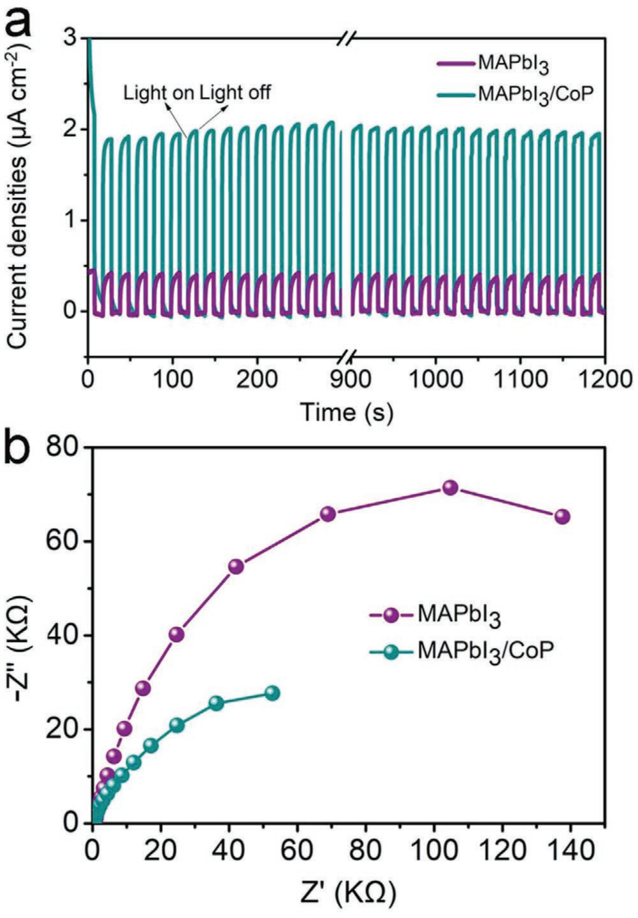

Figure 3. a) The transient photocurrent response curves of the $MAPbI_3$ and $MAPbI_3$/CoP hybrid. b) Nyquist plots of pristine $MAPbI_3$ and $MAPbI_3$/CoP hybrid.

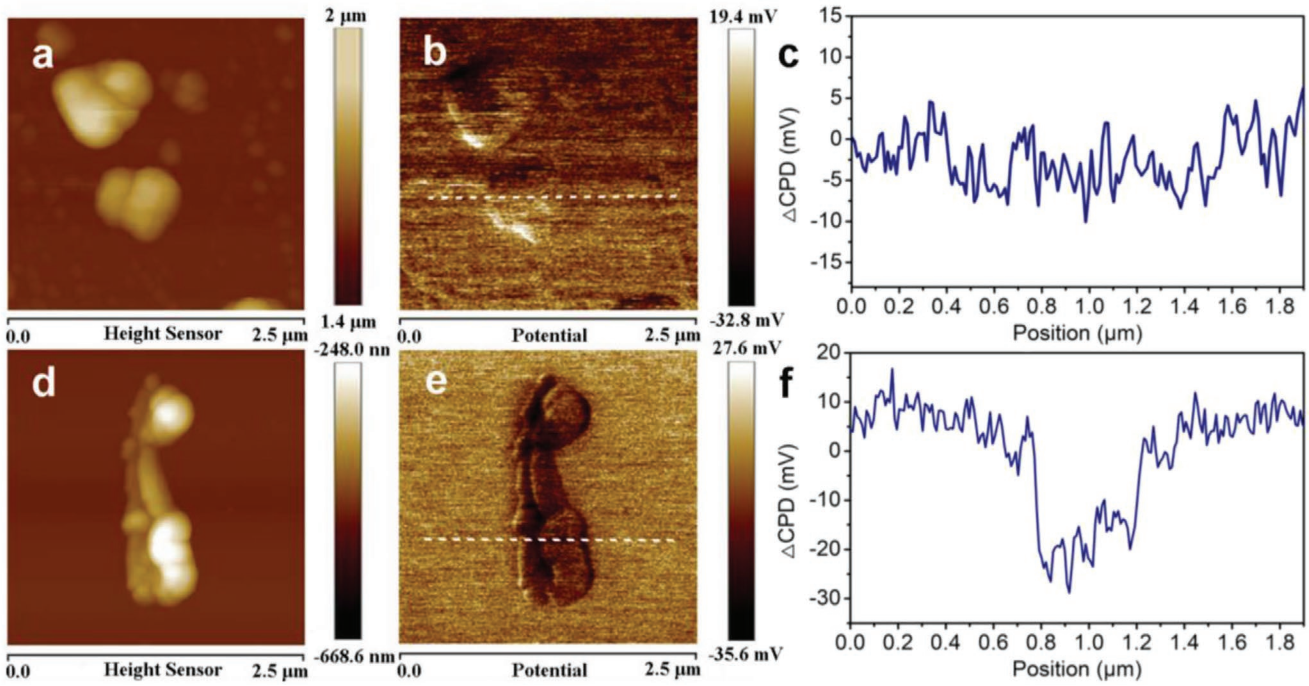

Figure 4. KPFM measurement of the pristine $MAPbI_3$ and $MAPbI_3$/CoP hybrid. a,d) AFM images. b,e) SPV images ($\Delta CPD = CPD_{light} - CPD_{dark}$). c,f) The corresponding line profiles of the SPV difference.

exhibits the chopped photocurrent curves of bare $MAPbI_3$ and $MAPbI_3$/CoP photoelectrodes recorded at the open-circuit potential. It can be found that $MAPbI_3$/CoP hybrid produces a photocurrent of ≈2.01 µA cm^{-2}, approximately fivefold larger than that of pristine $MAPbI_3$ (≈0.40 µA cm^{-2}), implying that the photoexcited charge carrier transfer in $MAPbI_3$/CoP hybrid is largely promoted. To further examine the charge transfer properties of the samples, the EIS plots were measured at 0 V versus Ag/AgCl electrode under simulated solar illumination (100 mW cm^{-2}, AM 1.5 G with a 420 nm cut-off filter). As shown in Figure 3b, a large semicircle in the testing frequency range is observed for the pristine $MAPbI_3$. By contrast, the $MAPbI_3$/CoP hybrid shows a drastically decreased semicircle after coupling with CoP, implying a more facilitated charge transfer and transportation process. The EIS results strongly confirm that the charge transfer property is obviously improved with the assistance of CoP co-catalyst, which is expected to obtain a better catalytic performance.

To further confirm the effective charge transfer and separation process in $MAPbI_3$/CoP hybrid, KPFM was performed to directly observe the spatial charge distribution of $MAPbI_3$/CoP heterojunction, as displayed in **Figure 4**. Note that this measurement is based on Au reference to probe the surface photovoltage (SPV) difference of samples before and after illumination. It can be found that no significant SPV signal changes are observed in the pristine $MAPbI_3$ due to the rapid charge carrier recombination. In contrast, a distinct negative signal is observed in the $MAPbI_3$/CoP hybrid, which could be attributed to the photogenerated electron accumulation on the surface of CoP particles under illumination. The potential difference of the $MAPbI_3$/CoP hybrid between the illumination and dark condition is ≈38.4 mV, which is significantly larger than that of pristine $MAPbI_3$ (≈6.3 mV). Such a remarkable difference in SPV signals between the $MAPbI_3$ and $MAPbI_3$/CoP samples strongly verifies the efficient spatial charge separation in the $MAPbI_3$/CoP hybrid.

In addition, the long-term photocatalytic activity of the $MAPbI_3$/CoP hybrid was also investigated and shown in **Figure 5**. It is worth noting that the H_2 yield rate for $MAPbI_3$/CoP hybrid increases with prolonging the photocatalytic reaction time. After continuous reaction of 27 h, the H_2 yield rate for $MAPbI_3$/CoP is 2087.5 µmol h^{-1} g^{-1}, which is ≈2.7 times larger than the value obtained after 3 h of reaction and is even superior to most of the reported $MAPbI_3$-based photocatalysts (Table S2, Supporting Information). Moreover, the recycling test of $MAPbI_3$/CoP hybrid also presents a similar trend with a gradually increased HER activity in five successive cycles (Figure S7, Supporting Information). To figure out the origin of this obviously increased H_2 evolution activity with the extension of reaction time, HRTEM images of samples after photocatalysis reaction were taken. As shown in Figure S8, Supporting information, both the lattice fringe of (202) face of $MAPbI_3$ and the lattice fringe of (201) face of CoP can be clearly observed, indicating both $MAPbI_3$ and CoP nanoparticles can maintain their crystalline structure. Furthermore, XRD patterns of the $MAPbI_3$/CoP hybrid with different photocatalytic reaction times were also determined (Figure S9, Supporting Information). It could be found that no significant phase structure changes are observed after long-term photocatalysis reaction except for a largely enhanced crystallinity of $MAPbI_3$, which implies a gradually improved charge transport properties as the photocatalytic reaction proceeding. Indeed, the EIS test of samples with different reaction times (Figure S10, Supporting Information) also confirms this improved charge transport

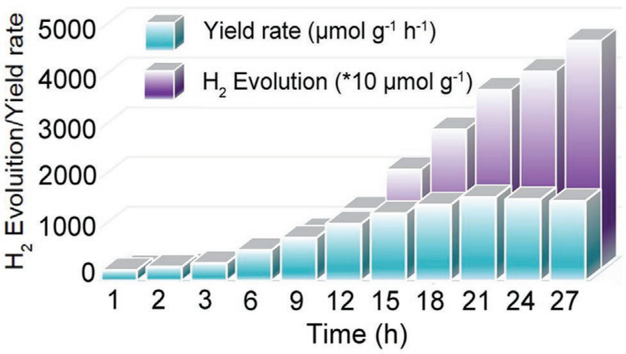

Figure 5. Long-term stability test of the $MAPbI_3$/CoP hybrid for photocatalytic H_2 evolution in $MAPbI_3$-saturated HI solution.

in the hybrid. In addition, the EDX analysis (Figure S3, Supporting Information) presents that the atomic percent of Co and P in $MAPbI_3$/CoP sample after 27 h of photocatalytic reaction is higher than that of the fresh one and the 3 h one, which reveals that more reaction active sites might be formed during the photocatalytic reaction process. Based on the aforementioned results, one can speculate that both the ripening of $MAPbI_3$ nanocrystals and the in situ photodeposition of CoP co-catalyst can promote the separation of photogenerated charge carriers and improve the interfacial catalysis kinetics, which may be responsible for the enhanced photocatalysis performances.

3. Conclusion

In summary, we reported an in situ photosynthesis of CoP co-catalyst on $MAPbI_3$ nanocrystal to construct an $MAPbI_3$/CoP heterojunction for efficient photocatalytic H_2 evolution. The H_2 evolution rate of the $MAPbI_3$/CoP hybrid was 785.9 $\mu mol\ h^{-1}\ g^{-1}$ after 3 h of reaction, which was about 8.0 times higher than that of pristine $MAPbI_3$. PL, TRPL, EIS, and KPFM results revealed that the transfer and separation of photogenerated charge carriers were significantly enhanced for the $MAPbI_3$/CoP hybrid sample, which should be responsible for the improved photocatalytic HER performance. Continuous long-term photocatalysis investigation indicated the photocatalytic HER performance increased with the reaction time, for example, H_2 amount of 56362.5 $\mu mol\ g^{-1}$ after 27 h of photocatalysis reaction, which can be probably ascribed to the improved crystallinity of $MAPbI_3$ and the more loading of CoP co-catalyst during the continuous photocatalysis reaction. Overall, this current study offers a facile in situ photosynthesis strategy to deposit metal phosphide co-catalyst on the surface of halide perovskite, which can be potentially broadened to various perovskite/co-catalyst hybrid materials for versatile photocatalytic applications, such as HER reaction, CO_2 reduction, dye degradation, and organic synthesis.

4. Experimental Section

Chemicals and Reagents: Oleic acid (OA), 50% H_3PO_2, absolute cobalt chloride ($CoCl_2$), and 30–33 wt% methylamine (MA) were purchased from Aladdin. Lead bromide (PbI_2) and $NaHPO_2$ powders were purchased from Sigma-Aldrich. Hydroiodic acid (HI, 57 wt%) and oleylamine (OAm) were purchased from Macklin. Hexane, chloroform, absolute ethanol, absolute diethyl ether, and dimethyl formamide (DMF) were purchased from Guangzhou Chemical Reagent Factory.

Fabrication of the $MAPbI_3$ Nanocrystal: $MAPbI_3$ nanocrystals were synthesized with modifications to the previously described method.[66,69,70] First, 62.5 mg (0.1 mmol) $MAPbI_3$ microcrystal powder was dissolved in 3 mL DMF with continuous stirring to form a $MAPbI_3$ precursor solution. Next, 200 μL oleic acid and 35 μL oleylamine were added into as above precursor solution. Third, 200 μL as-prepared perovskite precursor solution was added into 10 mL chloroform. After stirring for 3 h, the reaction mixture was centrifuged for 2 min at 9000 rpm, and the precipitate was collected. The resulting products were washed with hexane and chloroform in sequence two times, and then dried in a vacuum at 50 °C for 3 h.

Preparation of the $MAPbI_3$/CoP Hybrids, $MAPbI_3$ Films, and $MAPbI_3$/CoP Films: 2.5 mg as-prepared $MAPbI_3$ nanocrystal was added into a 40 mL photocatalytic bottle. Then 5 mL $MAPbI_3$-saturated HI solution with H_3PO_2 as the stabilizer was added. After that, 0.9 mg absolute cobalt chloride ($CoCl_2$) and 15 mg $NaHPO_2$ were added into the above mixture and sealed well. And then it was evacuated by a vacuum pump and treated with nitrogen atmosphere for 5 min, respectively. This process was repeated another time. Furthermore, the above mixture was illuminated under simulated sunlight without 420 nm cut-off filter for 30 min. The obtained precipitates were centrifuged, and subsequently rinsed with hexane. Finally, the product was dried in vacuum conditions at 50 °C.

The $MAPbI_3$ and $MAPbI_3$/CoP films were prepared by the centrifugally cast method. Briefly, FTO glass was cleaned ultrasonically in acetone for 30 min, rinsed with distilled water and absolute ethanol, and dried at 70 °C for 24 h. 2.5 mg $MAPbI_3$ or $MAPbI_3$/CoP hybrid was dispersed in 2 mL absolute diethyl ether, then ultrasound treated for 5 min. The suspension was centrifuged onto FTO at 9000 rpm for 2 min, and then dried at 50 °C under vacuum condition for 30 min to form the $MAPbI_3$ and $MAPbI_3$/CoP films.

Characterization and Measurements: The phase structure of samples was studied by X-ray powder diffraction (XRD; D-MAX 2200 VPC). The morphology and micro/nanostructure were investigated by the field-emission SEM (FE-SEM, Hitachi SU8010), TEM (JEOL-2010 HR), and aberration-corrected TEM (JEOL, ARM-200F). The thickness and spatial charge distribution were determined by AFM (DIMENSION FASTSCAN) and KPFM. The absorption behaviors were studied by the UV–vis spectrometer (Shimadzu UV-3600). The amount of evolved H_2 was qualitatively determined by using a gas chromatograph (GC9790, Fuli Analytical Instrument Co., Ltd.) equipped with a TDX-01 packed column and a TCD detector and N_2 was used as the carrier gas. Photoluminescence (PL) spectra were scanned on a photoluminescence spectrometer (FLS980, Edinburgh Instruments Ltd.), under an excitation wavelength of 500.0 nm. The PL decay spectra was recorded on the same instrument under a 472 nm laser extinction with the time-correlated single-photon counting mode. The decay curves were fitted using a biexponential decay kinetic function.

$$A(t) = K + A_1 e^{-\frac{t}{\tau_1}} + A_2 e^{-\frac{t}{\tau_2}} \tag{1}$$

where $A(t)$, A_1, and A_2 are constants obtained after fitting every decay curve. τ_1 and τ_2 reflect the fast and sloe decay components, respectively.[21,25] Based on the above decay fitting data, and the average PL life times (τ_{avg}) were calculated according to the following equation.

$$\tau_{avg} = \frac{B_1\tau_1^2 + B_2\tau_2^2}{B_1\tau_1 + B_2\tau_2} \tag{2}$$

Transient photocurrent responses and EIS were determined on the CHI660E electrochemical workstation and Zennium electrochemical workstation (Zahner) in a three-electrode configuration using dichloromethane solution containing 0.1 м tetrabutylammonium hexafluorophosphate as the electrolyte, respectively. The $MAPbI_3$ or the $MAPbI_3$/CoP film was employed as the working electrode, Pt mesh was used as the counter electrode and Ag/AgCl (saturated KCl) was used as the reference electrode.

Photocatalytic H_2 evolution was carried out in a 5 mL aqueous $MAPbI_3$-saturated HI solution with H_3PO_2 as a stabilizer. A 150 W Xe-lamp with a 420 nm cut-off filter was used as a visible-light source for the photocatalytic experiment. Typically, 2.5 mg $MAPbI_3$ nanocrystal was added into a 40 mL photocatalytic bottle. And 5 mL $MAPbI_3$-saturated HI solution with H_3PO_2 as a stabilizer was added into it. After that 0.9 mg absolute cobalt chloride ($CoCl_2$) and 15 mg $NaHPO_2$ were added into the above mixture and sealed well. And then it was evacuated by a vacuum pump, and treated with N_2 atmosphere for 5 min for two times. Furthermore, the above mixture was illuminated under visible light without 420 nm cut-off filter. After 30 min, it was evacuated by vaccuum pump and treated with N_2 atmosphere for 5 min. Finally, the photocatalytic experiment was illuminated under a 150 W Xe-lamp with 420 nm cut-off filter. The recycling catalytic experiments were carried out under the same condition but with the reaction system revacuumized by a vacuum pump and refilled with N_2 every 3 h. Five cycles (3 h for one cycle) were conducted.

Supporting Information

Supporting Information is available from the Wiley Online Library or from the author.

Acknowledgements

C.C. and Y.T. contributed equally to this work. The authors acknowledge the financial supports received from the National Natural Science Foundation of China (21875288), GDUPS (2016), the Guangdong Basic and Applied Basic Research Foundation (2019A1515110513), and the Fundamental Research Funds for the Central Universities (19lgjc07, 19lgzd24, and 20lgpy85).

Conflict of Interest

The authors declare no conflict of interest.

Keywords

cobalt phosphide, in situ photosynthesis, $MAPbI_3$ perovskites, nanocrystals, photocatalytic H_2 evolution

Received: February 17, 2020
Revised: May 17, 2020
Published online:

---

[1] Z. Y. Lin, C. Du, B. Yan, C. X. Wang, G. W. Yang, *Nat. Commun.* **2018**, *9*, 4036.
[2] Y. J. Zhang, Z. F. Xu, G. Y. Li, X. J. Huang, W. C. Hao, Y. P. Bi, *Angew. Chem., Int. Ed.* **2019**, *58*, 14229.
[3] M. Y. Xing, B. C. Qiu, M. M. Du, Q. H. Zhu, L. Z. Wang, J. L. Zhang, *Adv. Funct. Mater.* **2017**, *27*, 1702624.
[4] G. Zhou, Y. Shan, L. L. Wang, Y. Y. Hu, J. H. Guo, F. G. Hu, J. C. Shen, Y. Gu, J. T. Cui, L. Z. Liu, X. L. Wu, *Nat. Commun.* **2019**, *10*, 399.
[5] B. C. Qiu, Q. H. Zhu, M. M. Du, L. G. Fan, M. Y. Xing, J. L. Zhang, *Angew. Chem., Int. Ed.* **2017**, *56*, 2684.
[6] X. C. Wang, K. Maeda, A. Thomas, K. Takanabe, G. Xin, J. M. Carlsson, K. Domen, M. Antonietti, *Nat. Mater.* **2009**, *8*, 76.
[7] Z. M. Pan, G. G. Zhang, X. C. Wang, *Angew. Chem., Int. Ed.* **2019**, *131*, 7176.
[8] S. Park, W. J. Chang, C. W. Lee, S. Park, H.-Y. Ahn, K. T. Nam, *Nat. Energy* **2016**, *2*, 16185.
[9] Y.-F. Xu, M.-Z. Yang, B.-X. Chen, X.-D. Wang, H.-Y. Chen, D.-B. Kuang, C.-Y. Su, *J. Am. Chem. Soc.* **2017**, *139*, 5660.
[10] R. Prasanna, A. Gold-Parker, T. Leijtens, B. Conings, A. Babayigit, H. G. Boyen, M. F. Toney, M. D. McGehee, *J. Am. Chem. Soc.* **2017**, *139*, 11117.
[11] Y. Tong, B. J. Bohn, E. Bladt, K. Wang, P. Muller-Buschbaum, S. Bals, A. S. Urban, L. Polavarapu, J. Feldmann, *Angew. Chem., Int. Ed.* **2017**, *56*, 13887.
[12] H.-L. Wu, X.-B. Li, C.-H. Tung, L.-Z. Wu, *Adv. Mater.* **2019**, *31*, 1900709.
[13] J.-F. Liao, W.-Q. Wu, Y. Jiang, J.-X. Zhong, L. Z. Wang, D.-B. Kuang, *Chem. Soc. Rev.* **2020**, *49*, 354.
[14] Q. Q. Fan, G. V. Biesold-McGee, J. Z. Ma, Q. N. Xu, S. Pan, J. Peng, Z. Q. Lin, *Angew. Chem., Int. Ed.* **2020**, *59*, 1030.
[15] L. Li, Z. H. Sun, P. Wang, W. D. Hu, S. S. Wang, C. M. Ji, M. C. Hong, J. H. Luo, *Angew. Chem., Int. Ed.* **2017**, *56*, 12150.
[16] N. K. Kumawat, A. Swarnkar, A. Nag, D. Kabra, *J. Phys. Chem. C* **2018**, *122*, 13767.
[17] A. Swarnkar, V. K. Ravi, A. Nag, *ACS Energy Lett.* **2017**, *2*, 1089.
[18] T. Leijtens, K. A. Bush, R. Prasanna, M. D. McGehee, *Nat. Energy* **2018**, *3*, 828.
[19] L. Zhou, Y.-F. Xu, B.-X. Chen, D.-B. Kuang, *Small* **2018**, *14*, 1703762.
[20] H. Huang, H. Yuan, K. P. F. Janssen, G. Solís-Fernández, Y. Wang, C. Y. X. Tan, D. Jonckheere, E. Debroye, J. Long, J. Hendrix, J. Hofkens, J. A. Steele, M. B. J. Roeffaers, *ACS Energy Lett.* **2018**, *3*, 755.
[21] Y. Q. Wu, P. Wang, X. L. Zhu, Q. Q. Zhang, Z. Y. Wang, Y. Y. Liu, G. Z. Zou, Y. Dai, M.-H. Whangbo, B. B. Huang, *Adv. Mater.* **2018**, *30*, 1704342.
[22] X. M. Wang, H. Wang, H. F. Zhang, W. Yu, X. L. Wang, Y. Zhao, X. Zong, C. Li, *ACS Energy Lett.* **2018**, *3*, 1159.
[23] H. Wang, X. M. Wang, R. T. Chen, H. F. Zhang, X. L. Wang, J. H. Wang, J. Zhang, L. C. Mu, K. F. Wu, F. T. Fan, X. Zong, C. Li, *ACS Energy Lett.* **2019**, *4*, 40.
[24] Z. J. Zhao, J. J. Wu, Y.-Z. Zheng, N. Li, X. T. Li, X. Tao, *ACS Catal.* **2019**, *9*, 8144.
[25] R. Li, X. T. Li, J. J. Wu, X. D. Lv, Y.-Z. Zheng, Z. J. Zhao, X. Q. Ding, X. Tao, J.-F. Chen, *Appl. Catal. B* **2019**, *259*, 118075.
[26] Z. H. Guan, Y. Q. Wu, P. Wang, Q. Q. Zhang, Z. Y. Wang, Z. K. Zheng, Y. Y. Liu, Y. Dai, M.-H. Whangboc, B. B. Huang, *Appl. Catal. B* **2019**, *245*, 522.
[27] Z. J. Zhao, J. J. Wu, Y.-Z. Zheng, N. Li, X. T. Li, Z. L. Ye, S. Y. Lu, X. Tao, C. C. Chen, *Appl. Catal. B* **2019**, *253*, 41.
[28] H. Zhao, Y. X. Li, B. Zhang, T. Xu, C. Y. Wang, *Nano Energy* **2018**, *50*, 665.
[29] M. V. Pavliuk, M. Abdellah, J. Sá, *Mater. Today Commun.* **2018**, *16*, 90.
[30] Y. M. Guo, G. N. Liu, Z. X. Li, Y. B. Lou, J. X. Chen, Y. X. Zhao, *ACS Sustainable Chem. Eng.* **2019**, *7*, 15080.
[31] T. Wang, D. T. Yue, X. Li, Y. X. Zhao, *Appl. Catal. B* **2020**, *268*, 118399.
[32] Z. Z. Zhang, Y. Q. Liang, H. L. Huang, X. Y. Liu, Q. Li, L. X. Chen, D. S. Xu, *Angew. Chem., Int. Ed.* **2019**, *131*, 7341.
[33] Z. Z. Zhao, J. J. Wu, Y.-Z. Zheng, N. Li, X. T. Li, Z. L. Ye, S. Y. Lu, X. Tao, C. C. Chen, *Appl. Catal. B* **2019**, *253*, 41.
[34] M. Xiao, M. M. Hao, M. Q. Lyu, E. G. Moore, C. Zhang, B. Luo, J. W. Hou, J. L.-Duffn, L. Z. Wang, *Adv. Funct. Mater.* **2019**, *29*, 1905683.

[35] Y. J. He, Y. J. Yoon, Y. W. Harn, G. V. Biesold-McGee, S. Liang, C. H. Lin, V. V. Tsukruk, N. Thadhani, Z. T. Kang, Z. Q. Lin, *Sci. Adv.* **2019**, *5*, eaax4424.

[36] S.-H. Guo, J. Zhou, X. Zhao, C.-Y. Sun, S.-Q. You, X.-L. Wang, Z.-M. Su, *J. Catal.* **2019**, *369*, 201.

[37] M. V. Kovalenko, L. Protesescu, M. I. Bodnarchuk, *Science* **2017**, *358*, 745.

[38] A. Z. Pan, X. Q. Ma, S. Y. Huang, Y. S. Wu, M. J. Jia, Y. M. Shi, Y. Liu, P. H. Wangyang, L. He, Y. Liu, *J. Phys. Chem. Lett.* **2019**, *10*, 6590.

[39] L. Zhou, J.-F. Liao, Z.-G. Huang, X.-D. Wang, Y.-F. Xu, H.-Y. Chen, D.-B. Kuang, C.-Y. Su, *ACS Energy Lett.* **2018**, *3*, 2613.

[40] X.-D. Wang, N.-H. Miao, J.-F. Liao, W.-Q. Li, Y. Xie, J. Chen, Z.-M. Sun, H.-Y. Chen, D.-B. Kuang, *Nanoscale* **2019**, *11*, 5180.

[41] Y.-F. Xu, X. D. Wang, J. F. Liao, B. X. Chen, H. Y. Chen, D. B. Kuang, *Adv. Mater. Interfaces* **2018**, *5*, 1801015.

[42] Y.-F. Xu, M.-Z. Yang, H.-Y. Chen, J.-F. Liao, X.-D. Wang, D.-B. Kuang, *ACS Appl. Energy Mater.* **2018**, *1*, 5083.

[43] Z.-C. Kong, J.-F. Liao, Y.-J. Dong, Y.-F. Xu, H.-Y. Chen, D.-B. Kuang, C.-Y. Su, *ACS Energy Lett.* **2018**, *3*, 2656.

[44] L.-Y. Wu, Y.-F. Mu, X.-X. Guo, W. Zhang, Z.-M. Zhang, M. Zhang, T.-B. Lu, *Angew. Chem., Int. Ed.* **2019**, *58*, 9491.

[45] X.-D. Wang, Y.-H. Huang, J.-F. Liao, Y. Jiang, L. Zhou, X.-Y. Zhang, H.-Y. Chen, D.-B. Kuang, *J. Am. Chem. Soc.* **2019**, *141*, 13434.

[46] Y. Jiang, J.-F. Liao, H.-Y. Chen, H.-H. Zhang, J.-Y. Li, X.-D. Wang, D.-B. Kuang, *Chem* **2020**, *6*, 1.

[47] J. R. Ran, B. C. Zhu, S.-Z. Qiao, *Angew. Chem., Int. Ed.* **2017**, *56*, 10373.

[48] A. Y. Meng, L. Y. Zhang, B. Cheng, J. G. Yu, *Adv. Mater.* **2019**, *31*, 1807660.

[49] J. R. Ran, H. L. Wang, H. Y. Jin, C. Y. Ling, X. L. Zhang, H. X. Ju, L. Q. Jing, J. L. Wang, R. K. Zheng, S.-Z. Qiao, *J. Mater. Chem. A* **2018**, *6*, 23278.

[50] H. B. Zhang, P. Zhang, M. Qiu, J. C. Dong, Y. F. Zhang, X. W. Lou, *Adv. Mater.* **2018**, *31*, 1804883.

[51] J. G. Ran, M. Jaroniec, S.-Z. Qiao, *Adv. Mater.* **2018**, *30*, 1704649.

[52] Y.-X. Chen, Y.-F. Xu, X.-D. Wang, H.-Y. Chen, D.-B. Kuang, *Sustainable Energy Fuels* **2020**, *4*, 2249.

[53] J.-F. Liao, Y.-T. Cai, J.-Y. Li, Y. Jiang, X.-D. Wang, H.-Y. Chen, D.-B. Kuang, *J. Energy. Chem.* **2020**, https://doi.org/10.1016/j.jechem.2020.04.017.

[54] J. Kibsgaard, C. Tsai, K. Chan, J. D. Benck, J. K. Nørskov, F. Abild-Pedersen, T. F. Jaramillo, *Energy Environ. Sci.* **2015**, *8*, 3022.

[55] T. T. Liu, K. Y. Wang, G. Du, A. M. Asiric, X. P. Sun, *J. Mater. Chem. A* **2016**, *4*, 13053.

[56] J. Q. Tian, Q. Liu, A. M. Asiri, X. P. Sun, *J. Am. Chem. Soc.* **2014**, *136*, 7587.

[57] C. Zhang, Y. Huang, Y. F. Yu, J. F. Zhang, S. F. Zhuo, B. Zhang, *Chem. Sci.* **2017**, *8*, 2769.

[58] G. Y. Zhou, M. Li, Y. L. Li, H. Dong, D. M. Sun, X. E. Liu, L. Xu, Z. Q. Tian, Y. W. Tang, *Adv. Funct. Mater.* **2019**, *30*, 1905252.

[59] T. T. Liu, L. S. Xie, J. H. Yang, R. M. Kong, G. Du, A. M. Asiri, X. P. Sun, L. Chen, *ChemElectroChem* **2017**, *4*, 1840.

[60] T. T. Liu, D. Liu, F. L. Qu, D. X. Wang, L. Zhang, R. X. Ge, S. Hao, Y. J. Ma, G. Du, A. M. Asiri, L. Chen, X. P. Sun, *Adv. Energy Mater.* **2017**, *7*, 1700020.

[61] R. Zhang, X. Ren, S. Hao, R. X. Ge, Z. A. Liu, A. M. Asiri, L. Chen, Q. J. Zhang, X. P. Sun, *J. Mater. Chem. A* **2018**, *6*, 1985.

[62] B. C. Qiu, Q. H. Zhu, M. Y. Xing, J. L. Zhang, *Chem. Commun.* **2017**, *53*, 897.

[63] Q. S. Liang, F. B. Shi, X. F. Xiao, X. F. Wu, K. K. Huang, S. H. Feng, *ChemCatChem* **2018**, *10*, 2179.

[64] X. Z. Yue, S. S. Yi, R. W. Wang, Z. T. Zhang, S. L. Qiu, *Small* **2017**, *13*, 1603301.

[65] B. Luo, R. Song, J. F. Geng, X. H. Liu, D. W. Jing, M. L. Wang, C. Cheng, *Appl. Catal. B* **2019**, *256*, 117819.

[66] J.-F. Liao, Y.-X. Chen, J.-H. Wei, Y.-T. Cai, X.-D. Wang, Y.-F. Xu, D.-B. Kuang, *Nano Res.* **2019**, *12*, 2640.

[67] T. Wang, H. F. Zhang, S. M. Hou, Y. Zhang, Q. J. Li, Z. L. Zhang, H. P. Gao, Y. L. Mao, *Nanomaterials* **2019**, *9*, 1660.

[68] P. F. Wang, S. H. Zhan, H. T. Wang, Y. G. Xia, Q. L. Hou, Q. X. Zhou, Y. Li, R. R. Kumar, *Appl. Catal. B* **2018**, *230*, 210.

[69] L. Protesescu, S. Yakunin, S. Kumar, J. Bar, F. Bertolotti, N. Masciocchi, A. Guagliardi, M. Grotevent, I. Shorubalko, M. I. Bodnarchuk, *ACS Nano* **2017**, *11*, 3119.

[70] F. Zhang, S. Huang, P. Wang, X. M. Chen, S. L. Zhao, Y. P. Dong, H. Z. Zhong, *Chem. Mater.* **2017**, *29*, 3793.